

---

## A robotic system for radioactive seeds implantation in hepatocellular carcinomas: mechanism and control

First Author · Second Author

Received: date / Accepted: date

**Abstract Purpose** Radioactive seeds implantation is an effective invasive treatment method for malignant liver tumors in hepatocellular carcinomas. This paper aims to develop a robotic system in assisting surgeons in operating, which is characterized by high-accuracy, multiple degrees of freedom and multimodal feedback.

**Method** The robotic system consists of a seven-degrees-of-freedom actuator with axial force sensor, an ultrasound(US) scanner and an optical tracking system. To ensure the safety of the system, a control strategy and a path planning algorithm based on improved artificial potential field approach are introduced to it. Experiments were performed to determine positioning and orientating accuracy as well as validate the path planning procedure of the system.

**Result** The accuracy of positioning with and without rotation was  $0.66 \pm 0.49 \text{ mm}$  and  $0.88 \pm 0.49 \text{ mm}$ . Orientating accuracy was  $\pm 0.2$  degree for  $\theta_4$  and  $\pm 0.1$  degree for  $\theta_5$ . Needle placement accuracy was  $1.1 \pm 0.5 \text{ mm}$ . The feasibility of the path planning algorithm is demonstrated by simulation and motion planning experiments based on an abdominal phantom.

**Conclusion** This paper presents a robotic system with force and US image feedback in assisting surgeons performing brachytherapy of liver tumors. The proposed robotic system is capable of executing an accurate needle insertion task while avoiding collision between obstacles and the robot. To further evaluate the accuracy of the robotic system, more experiments on phantom and in-vivo need to be performed in future works.

**Keywords** Robotics · Brachytherapy · hepatocellular carcinomas · Path-planning

---

F. Author  
first address  
Tel.: +123-45-678910  
Fax: +123-45-678910  
E-mail: fauthor@example.com

S. Author  
second address

## 1 Introduction

Liver cancer has been regarded as the 6<sup>th</sup> most commonly diagnosed cancer and 4<sup>th</sup> leading cause of cancer death worldwide in 2018, which contributes over 841,000 new cases and 782,000 deaths. The bulk of primary liver cancer is hepatocellular carcinomas (HCC), which comprises 75% to 85% of cases [1]. There are already some effective therapies about HCC and have greatly improved the patients' survival rate, including percutaneous ethanol injection (PEI), transarterial chemoembolization (TACE), radiofrequency ablation (RFA) [2]. Recently, 125-iodine seeds implantation (**Fig.1**) shows promising therapeutic effects on the treatment of malignant liver tumors in HCC [3]. It can release low-dosage X-ray and increase the dosage distribution ratio between locally radioactive tissues and normal tissues. The therapy has also been proven to have advantages in relieving short-term pain and improving the quality of life for patients [4]. Therefore, 125-Iodine seed implantation is regarded as a relatively safe and effective therapy in treating cancer with tumors [5]. In application, the treatment, however, may bring about the following difficulties: 1) the efficacy of the technique relies on the precision of needle placement. 2) radiation exposure to physicians may cause irreversible damage to them. 3) costa and lung tissue are always kinds of obstacles in surgery. Besides, it's also an underlying problem with the movement of the liver caused by breathing, which makes the tumor tracking difficult [6, 7]. To provide stable needle manipulation, as well as increasing the accuracy, dexterity and repeatability of the surgery, surgical robots with medical image guide may be better candidates for the implantation of 125-Iodine seeds [8].

There have been substantial works in the image-guided needle guide robotic



Fig. 1: Radioactive seeds implantation in HCC

system for liver intervention. For Magnetic Resonance Imaging (MRI) guided only, Franco et al. [9, 10] presented a 4-Degrees-of-Freedom (DoF) magnetic resonance imaging (MRI) based needle guiding robot. The needle actuated unit is mounted on a fixed gantry and provides 2-DoF rotation with 2-DoF translation by four pneumatic plastic cylinders on it. A marker is attached to the needle guide for robot registration under MRI in surgery. Song et al. [11] designed a two rotational joints structure-based

MRI-guided robotic needle guidance device for liver interventions. The registration of the needle orientation and insertion device is also based on MR-visible markers embedded in it. Another MRI based needle guiding systems for liver intervention [12, 13] also provide multi-DoF for actuating needle and markers for registration. For Computed Tomography (CT) guided only, Arnolli et al. [14] used a CT-guided Demcon Needle Placement System (NPS) to provide 2-DoF orientation as well as 6-DoF pneumatic-hydraulic locking module of the needle. A user interface based on MATLAB is applied to the system for needle trajectory planning and real-time visual feedback in surgery. Shah et al. [15] developed a needle driven robotic system named 'AcuBot1 V2-RND' with joints to spin and release the needle. The system was equipped with two force sensors, which make insertion force measuring possible. The two systems can be used for both ablation of liver tumors and lung nodule biopsies. For US-guided only, Kobayashi et al. [16] proposed a 3-DoF needle insertion manipulator with a US-probe providing position information of the needle tip, which decreases registration error. Boctor et al. [17] developed a 3D US-guided robotic needle placement system for RFA of liver tumors. The system consists of a surgical workstation, 2D US system and needle driven robot, with a magnetic tracking system tracking the robot in surgery. Orhan et al. [18] designed a 2D-US guided robot with 5-DoF for doing general biopsies on humans. They both used optical tracking system (OTS) and encoder data from motors to calibrate the end effector.

Most of the robotic systems mentioned above are for RFA or biopsies. As for radioactive seeds implantation robotic systems, recently, several research groups have proposed their works on it. Ma et al. [19] reported an auto-positioning system for templates with robot assisting. Instead of traditional positioning methods, the system calculates the target position of the template from patients' preoperative CT scanning, then sends the position to the robot-assisted system for adjusting the template. Finally, the needle was inserted and 125-I seeds were implanted by clinicians manually. Zequn et al. [20, 21] developed a robotic system for brachytherapy of, with 7-DoF manipulator KUKA iiwa 14 (KUKA, Germany) and seeds implantation end tool. The system is equipped with force/optical feedback and has a systematic strategy for calibrating the robotic system. Zhu et al. [22, 23] put forward a novel 6-DoF arch-like structure for needle orienting, with an end effector of seeds' delivering on it. The system has its trajectories planning and needle positioning by preoperative CT scanning, and its motion-tracking by OTS.

However, the frameworks of Zequn et al. and Zhu et al. are short of real-time feedback from patients, which makes it difficult to monitor the real-time environment under the skin in surgery. Jiang et al. [24] integrated real-time US image guidance into their work. Their robotic system has 9-DoF, where 3-DoF for platform position adjustment, 2-DoF for probe adjustment and 4-DoF for manual template adjustment. Nevertheless, the system lacks force feedback during needle insertion. Meanwhile, the implantation of seeds is also executed by physicians.

In this paper, we present a 7-DoF robotic system with axial force and US image feedback for radioactive seeds implantation in HCC. The main contributions are as follows: 1) A novel mechanical structure and method for registration of the robotic system for realizing robot-assisted surgery are proposed. The robotic system provides surgeons with high-accuracy operating and keeps them from the radiation of

the seeds; 2) Obstacles avoiding path planning algorithm based on improved artificial potential field approach is introduced in the surgical planning of the system. Both pre-operative CT image and intra-operative registraion are used to avoid colliding the patient and the important tissue in abdomen. 3) The robotic system feeds all axial force of the needle, US image of the patient and position of the end effector back to surgeons. These multimodal information can be further utilized to design safety strategy and intra-operative compensate on the movement of the liver. 4) An experimental platform is developed, which can be used for validating control algorithm or performing phantoms/animals experiment.

This paper is organized as follows. Sect. 2 presents the detail about the proposed method and material. In this section, Sect. 2.1 first discusses the design requirement on the robotic system. The mechanical design is presented in Sect. 2.2. To control the robotic system, we analyze the forward and inverse kinematics of the system in Sect. 2.1 and Sect. 2.4, and present an obstacle-avoiding path planning algorithm based on improved artificial potential field approach in Sect. 2.4.3. In Sect. 2.5, the clinical workflow and methods of intra-operative registration are described. The performance of the robotic system on accuracy and motion planning is presented and evaluated in Sect. 3. Sect. 4 analyzes and concludes this paper with suggestions for future work.

## 2 Method and material

### 2.1 Design requirement

To reproduce the manual procedure, the robotic system demands at least 5 DoF, where three axes for translation and two axes for needle rotation, as shown in **Fig.2** [25]. In radioactive seeds implantation, high stiffness needles are always used for implanting seeds (eg. 18 Gauge needles), which makes it hard to curve when inserting. Thus we assume that the needle used in the robotic system is a rigid body. It means the rotation of the needle will not contribute to its orientation.

As for adult patients without hepatic diseases, the hepatic height is likely to be

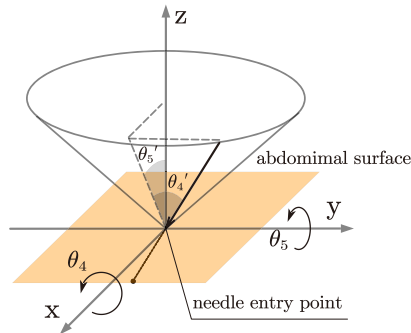


Fig. 2: Workspace requirement analysis

160 mm and the width to be 210 mm on coronal plane [26, 27], which means the robotic workspace on the coronal plane should larger than  $210 \times 160 \text{ mm}^2$ . Besides, to obtain enough feedback both on the robotic system and patients, OTS and real-time 2D US image feedback to the operators are required on it. Tracking systems like OTS can provide both real-time position and orientation information, which can be used for registration and position feedback of the robotic system. Real-time 2D US image can feed the environment under the skin back to surgeons, which provides a safe and rapid means for abdominal puncture [28].

Last but not least, for the sake of safety, the robotic system should be equipped with force feedback, which can prevent the robot from encountering situation in which abnormal force occurs when inserting.

## 2.2 Mechanism design

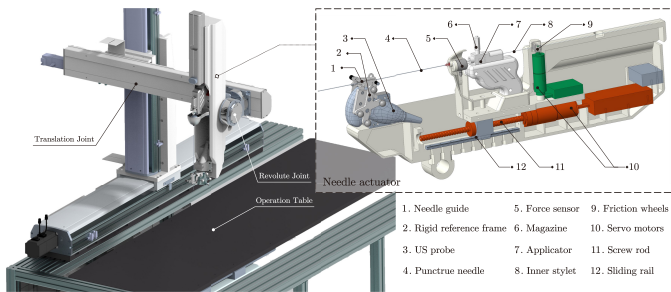


Fig. 3: Mechanism overview of the robotic system

To ensure that the system has enough degrees of freedom, three axes translation joints and two axes revolute joints are used. The translation joints are driven by Delta Servo System (ASDA-B2 Series, Delta Electronics, China), providing the robotic system with large workspace to place the end effector ( $527.5 \times 750 \times 603.4 \text{ mm}^3$ ). The revolute joints are driven by two servo motors (HT-03, Hai Tai Electromechanical Equipment, China) with high continuous torque 6.9NM. Together with the translation joints, which have maximum loading of 15kg on the 3rd arm, the high continuous torque involves redundant capability of driving the needle actuator, making high-load and long-time running of the robotic system possible.

The needle actuator is comprised of multiple components and is driven by a two-DoF Maxon Servo System (Maxon motor AG, Switzerland), one for needle insertion and the other for seeds implantation, as is shown in Fig.3. For needle insertion, the linear motion is driven by motorized screw and sliding rail, ensuring the stable and continuous control of puncture needle. The needle is fixed to a disposable part attached to the force sensor (SBT671, SIMBATOUCH, China), which can measure the axial force suffered by the needle in operation. The inner stylet is driven by a pair of friction wheels made by silicon. The friction wheels are also aseptic and disposable,

which can be replaced after finishing operation. A rigid reference frame is fixed on the needle guide for calibration, which will be further discussed in Sect. 2.5.

### 2.3 Forward kinematics

**Fig.4** is a schematic of the kinematic model of the robotic system, where the end-effector is the tip of the needle. The model is comprised of four prismatic joints and two revolute joints, except for the seeds implantation joint. Link parameters are assigned based on modified Denavit-Hartenberg convention [29], which is shown on Table 1.

The transformation matrix of the end effector concerning the base of the robot

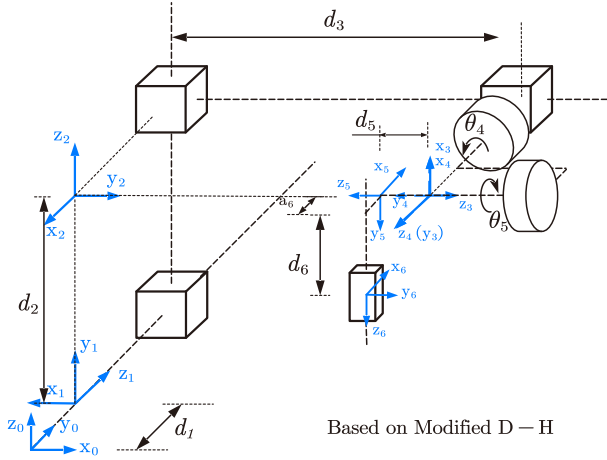


Fig. 4: Schematic representation of robot's kinematics

Table 1: D-H parameters of each joint

i	$a_{i-1}$	$\alpha_{i-1}$	$d_i$	$\theta_i$
1	0	-90	$d_1$	180
2	0	-90	$d_2$	90
3	0	-90	$d_3$	-90
4	0	-90	0	$\theta_4$
5	0	-90	$d_5$	$\theta_5 + 90$
6	$a_6$	-90	$d_6$	0

can be obtained by the homogenous matrix of each link. In particular,  ${}^{Robot0}T_{Robot5}$  (Equation(1)) is shown separately for the need of computation scheme, which will be

further discussed later.

$${}_{Robot0}T_{Robot5} = \begin{bmatrix} -c\theta_5's\theta_4 & s\theta_4s\theta_5' & -c\theta_4 & d_3 - d_5 \cdot c\theta_4 \\ s\theta_5' & c\theta_5' & 0 & d_1 \\ c\theta_4c\theta_5' & -c\theta_4s\theta_5' & -s\theta_4 & d_2 - d_5 \cdot s\theta_4 \\ 0 & 0 & 0 & 1 \end{bmatrix} \quad (1)$$

Where  $\theta_5' = \theta_5 + 90^\circ$ ,  $c = \cos()$ ,  $s = \sin()$ ,  $\{\text{Robot } i\}$  means the coordinate system of joint  $i$ .

## 2.4 Inverse kinematics

The design of the manipulator eases the inverse kinematics computation. In robot-assisted surgery, it's of great importance to concern about the safety of robotic motion, especially the collision between the robot and patient. For the sake of safety, we'd like to define control strategy before its inverse kinematics computation.

### 2.4.1 Control strategy in path planning

Once we have a target point (TP) in the tumor and the expected orientation of puncture, the robotic system will find a path to align the needle to the orientation and feed the tip to TP. However, it is dangerous for the end effector to move to TP directly, since the probe should attach to the skin surface in a suitable orientation, and the collision between the end effector and patient should be avoided. Hence, we designed a control strategy on path planning as shown in Fig.5, in which the path planning will undergo three steps:

- 1) The end effector is initialized at the original position (base point, BP), and move to the feeding point (FP) through the trajectory planning algorithm.
- 2) After reaching FP, the robotic system will feed the probe along with the expected orientation, until it arrives at the contact point (CP), which means the probe fully contact with the skin surface.
- 3) Finally, after the confirmation of the operator, the system starts puncturing under the monitoring of US. When the tip of the needle reaches TP, the seeds implantation tool will implant a radioactive seed at TP. The FP is defined as the goal point in path planning instead of CP makes the motion of manipulator safer. Besides, it's more reasonable for a US probe moving to the skin surface in such direction.

### 2.4.2 Computation scheme

The robotic system includes 4 spaces: robot space, patient's space, optical tracking space and CT 3D reconstruction space. The system is described under 6 coordinate systems: The optical positioning coordinate system  $\{O\}$ , 3D phantom model's coordinate system  $\{C\}$ , robotic base coordinate system  $\{Robot0\}$ , the end effector coordinate system  $\{E\}$ , the passive markers frame on US probe  $\{M\}$  and patient's coordinate system  $\{S\}$ , as shown in **Fig.6**.

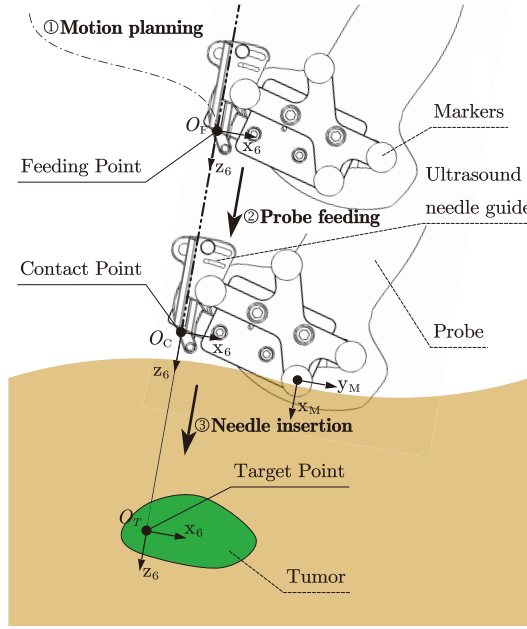


Fig. 5: Control strategy: The end effector first arrives at Feeding point, then moves along the inserting orientation, finally reaches contact point and inserts needle

In robot space, for a given target  $P_T(x_T, y_T, z_T)$  and its orientation  $(\theta_{4T}, \theta_{5T})$ , such as FP or CP, the transformation matrix  ${}^0T_T$  between target and BP can be calculated [30]. As is described in Sect. 2.4.1, motion planning in the first two steps uses only 5-DoF of the robotic system, except for the 6<sup>th</sup>-DoF for needle insertion. Therefore, we defined a fixed point E as the end effector at the exit of the needle guide, which is shown up as  $O_F$  and  $O_C$  in Fig.5 and {E} in Fig.6. As for the fixed point, it can be regarded as an offset from Joint 5 to Joint 6 and facilitates the path planning computation. At this point,  ${}^{Robot5}T_E$  is a constant matrix. Variables including  $d_1, d_2, d_3, \theta_4, \theta_5$  can be obtained based on the equation (2):

$${}^0T_T({}^{Robot5}T_E)^{-1} = {}^{Robot0}T_{Robot5} \quad (2)$$

When it's in optical tracking space, given a target point and entry point like FP and CP in {O}, the matrix  ${}^0T_{FP}$  can be obtained. Then the variables can be deduced as shown in (3):

$$({}^{Robot5}T_E)^{-1}({}^0T_{Robot0})^{-1}{}^0T_{FP} = {}^{Robot0}T_{Robot5} \quad (3)$$

Where  ${}^0T_{Robot0}$  represents the transformation matrix between the coordinate system of {Robot0} to {O}, and the matrix can be obtained through registration before surgery. The matrix  ${}^{Robot0}T_{Robot5}$  is shown on Equation (1).

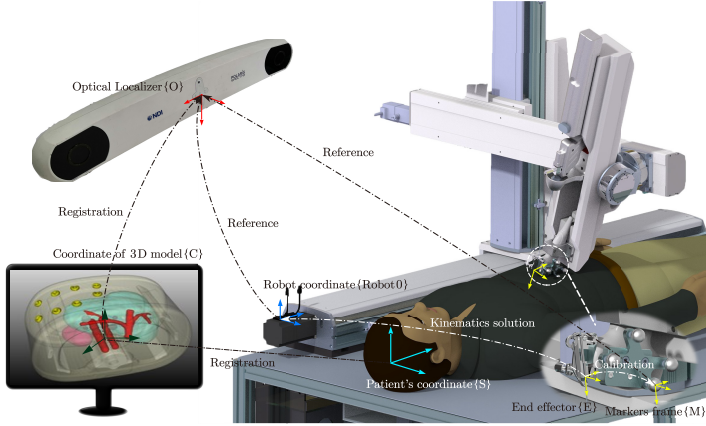


Fig. 6: Relationships between each coordinate system

#### 2.4.3 Artificial Potential Field Approach in motion planning

Considering the collision between robot and patients, we introduced an improved artificial potential field approach (Improved-APF) [31] to motion planning. After the registration of patients' pre-operative CT-image before an operation, point cloud generated by the model is mapped to the coordinate system  $\{O\}$ , which is defined as obstacles relative to the robotic system. To avoid colliding with these obstacles, the trajectory in motion planning is generated by Improved-APF, where the attractive potential function and attractive force are shown on (4)(5).

$$U_{att}(\mathbf{q}) = \frac{1}{2} \varepsilon \rho^2(\mathbf{q}, \mathbf{q}_{goal}) \quad (4)$$

$$\mathbf{F}_{att}(\mathbf{q}) = -\nabla U_{att}(\mathbf{q}) = \varepsilon (\mathbf{q}_{goal} - \mathbf{q}) \quad (5)$$

Where,  $\varepsilon$  is a positive scaling factor, and  $\rho(\mathbf{q}, \mathbf{q}_{goal})$  is the distance between the end effector and the goal position.

As for the planning in this system, the goal position is always close to obstacles, which will bring about goals non-reachable problem. Therefore, we used an improved repulsive potential function proposed in [31], as shown in (6).

$$U_{rep}(\mathbf{q}) = \begin{cases} \frac{1}{2} \eta \left( \frac{1}{\rho(\mathbf{q}, \mathbf{q}_{obs})} - \frac{1}{\rho_0} \right)^2 \rho^n(\mathbf{q} \cdot \mathbf{q}_{goal}) & \text{if } \rho(\mathbf{q} \cdot \mathbf{q}_{obs}) \leq \rho_0 \\ 0 & \text{if } \rho(\mathbf{q} \cdot \mathbf{q}_{obs}) > \rho_0 \end{cases} \quad (6)$$

Where  $\eta$  is a positive scaling factor,  $\rho_0$  is a positive constant denoting the distance of influence of the obstacle. The corresponding repulsive force is given by

$$\begin{aligned}\mathbf{F}_{rep}(\mathbf{q}) &= -\nabla U_{rep}(\mathbf{q}) \\ &= \begin{cases} F_{rep1}\mathbf{n}_{OR} + F_{rep2}\mathbf{n}_{RG} & \text{if } \rho(\mathbf{q} \cdot \mathbf{q}_{obs}) \leq \rho_0 \\ 0 & \text{if } \rho(\mathbf{q} \cdot \mathbf{q}_{obs}) > \rho_0 \end{cases}\end{aligned}$$

Where

$$F_{rep1} = \eta \left( \frac{1}{\rho(\mathbf{q} \cdot \mathbf{q}_{obs})} - \frac{1}{\rho_0} \right) \frac{\rho^n(\mathbf{q} \cdot \mathbf{q}_{goal})}{\rho^2(\mathbf{q} \cdot \mathbf{q}_{obs})} \quad (7)$$

$$F_{rep2} = \frac{n}{2} \eta \left( \frac{1}{\rho(\mathbf{q} \cdot \mathbf{q}_{obs})} - \frac{1}{\rho_0} \right)^2 \rho^{n-1}(\mathbf{q} \cdot \mathbf{q}_{goal}) \quad (8)$$

$\mathbf{n}_{OR} = \nabla \rho(\mathbf{q}, \mathbf{q}_{obs})$  and  $\mathbf{n}_{RG} = -\nabla \rho(\mathbf{q}, \mathbf{q}_{goal})$  are two unit vectors pointing from the obstacle to the end effector and from the robot to the goal, respectively.

## 2.5 Interventional path planning framework

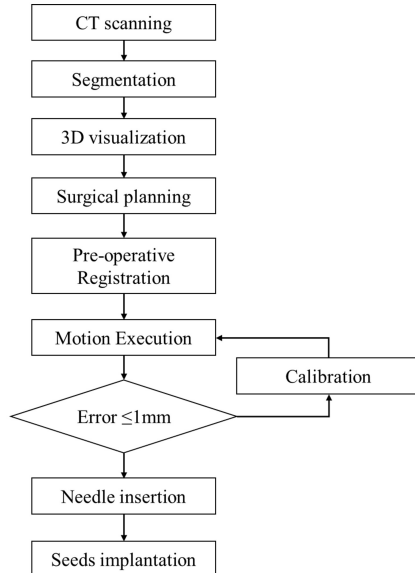


Fig. 7: Surgical workflow

The clinical workflow that we have designed for our robotic system is shown in the block diagram in **Fig.7**. Before CT scanning, several markers were attached to the surface of the abdomen for image registration. After CT scanning, the organs and

tumors were manually segmented with the open-source software 3D Slicer. With the segmentation and reconstruction, a 3D model of the abdomen with skin, ribs, vessels, liver and tumor was created. To implant radioactive seeds into a tumor, the distribution including the positions and orientations of it was calculated and manually defined by the radiologists. Then the positions of the seeds were regarded as a series of target volumes in the tumor's model and the entry volume where needle puncture on the skin surface was defined by the orientation from the target volumes. Finally, the needle path was determined by the two volumes from the skin surface to the tumor in CT 3D reconstruction space.

To find the pose transformation matrix of the coordinate systems in **Fig.6**, several methods were carried out:

- 1) With markers on the abdomen of the patient, the transformation matrix of  $\{S\}$  relative to  $\{O\}$  can be obtained by registration through pointing stylus (standard Polaris stylus, Northern Digital Inc., Waterloo, ON, Canada) to the markers. After recording the positions of these markers in  $\{O\}$ , we used the iterative closest point (ICP) algorithm [32] to match the two point sets between  $\{O\}$  and  $\{S\}$ , then the transformation matrix of  $\{S\}$  relative to  $\{O\}$  was computed. As the transformation of  $\{S\}$  with respect to  $\{C\}$  can be computed in model, the relationship between  $\{C\}$  and  $\{O\}$  can be described by  ${}^O T_C = {}^O T_S {}^S T_C$ .
- 2) To obtain the pose transformation matrix of  ${}^O T_{Robot0}$ , a passive rigid reference frame is fixed on the body of the first translational joint, thus the matrix  ${}^O T_{Robot0}$  can be measured directly.
- 3) Put the deformation of the robotic system into consideration, although the position and orientation of  $\{E\}$  can be computed by kinematics solution, it may have some-what deviation. Therefore, a passive markers frame was attached to the needle-guide. With the frame, it can measure the real-time position and orientation matrix  ${}^O T_M$  of the frame  $\{M\}$  relative to  $\{O\}$ , which can in turn act as feedback to calibrate the robotic system.

Both encoders in motors and OTS are used to ensure the accuracy of robotic motion control. Taking the patient into consideration, we use US image to provide image feedback to the surgeon for the sake of intra-operative safety. When performing operation, the movement of the end effector is visualized on the graphical user interface (**Fig.8**) according to the position of the rigid reference frame on the probe. The US image is also shown on the screen for monitoring the environment under the skin in real time. With the feedback of the US image, the operator can adjust the end effector for a more suitable position/orientation.

### 3 Experiment result and evaluation

We conducted experiments to evaluate the computing procedure as well as the accuracy of motion control. Then we validated the performance of the trajectory planning algorithm on an abdominal phantom (**Fig.9**).

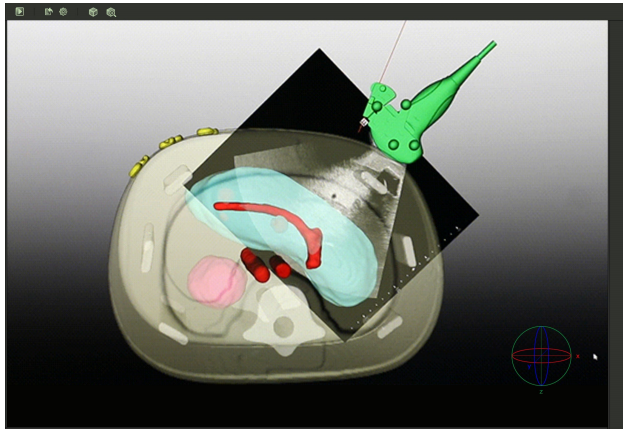


Fig. 8: Graphical user interface



Fig. 9: Experiment setup

### 3.1 End effector positioning and orientating experiment

To evaluate the accuracy of the positioning and orientating about  $\{E\}$ , a series of targeting experiments were performed. In these experiments, a rigid reference frame was placed on the table, whose transformation matrix concerning  $\{O\}$  was measured in real-time. As is described in Sect. 2.4.1, given two points like TP and CP in  $\{O\}$ , we can obtain the expected position and orientation of  $\{E\}$  relative to  $\{O\}$ . The two points were defined in the local coordinate system of the fixed rigid reference frame. To evaluate the error of the accuracy, after the end effector arriving at the expected position, position of the end effector (Point A) and a point on the needle (Point B) in  $\{O\}$  were recorded by the stylus (**Fig.10a**). Euclidean distance

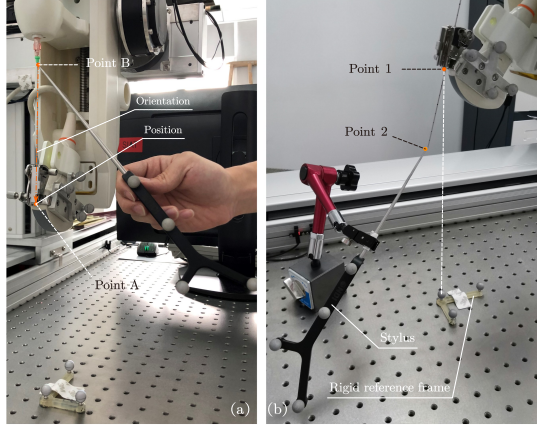


Fig. 10: Accuracy experiments:(a)Two points measured for evaluating the position and orientation of the end effector;(b)The robotic system stopped at Point 1 and inserted its needle to Point 2

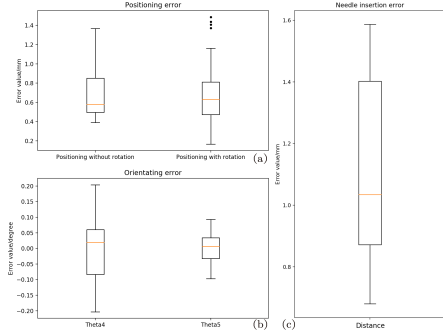


Fig. 11: The maximum, minimum, median errors of (a) positioning and (b) orientating experiments;(c)Distance between two needles' tip

$(\sqrt{\Delta X^2 + \Delta Y^2 + \Delta Z^2})$  between the former point and expected position in  $\{O\}$  was defined as positioning error (PE) [22]. As for the later, Orientating error (OE) was defined as the difference between the orientation ( $\theta_4, \theta_5$ ) calculated by the two points and the expected orientation. We sampled 60 points in robot's workspace, where 20 points for translation without rotation and 40 points for translation with rotation. The results were shown in **Fig.11a,b**. The results showed that the PE in our system was less than 2 mm and the OE in our system was less than  $\pm 0.5$  degree.

We also conducted experiments to test the accuracy of needle insertion, as shown in **Fig.10b**. Point 1 was defined in the local coordinate system of the fixed rigid reference frame above the optical table, and the other point was defined at the tip of the stylus. The end effector should move to the Point 1 and inserting its needle to the Point 2. After the robotic system finished the motion, the distance between the needle

tip and stylus's tip was recorded manually. The result was shown in **Fig.11c**, where 10 points were sampled to evaluated the inserting accuracy.

### 3.2 Motion planning experiment

To evaluate the performance of the trajectory planning algorithm, an abdominal phantom (Model 057A, Cirs, USA) with eight markers (#128, BEEKLEY Medical, USA) was used in the experiment, as is shown on **Fig.9**.

After CT scanning and 3D reconstruction of the phantom, we selected a target

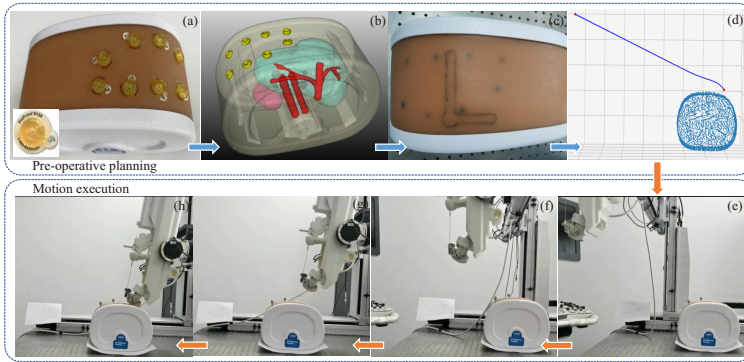


**Fig. 12: Pre-operative planning:**(a)Abdominal phantom with eight markers;(b)3D model of the phantom after CT scanning and reconstruction;(c)Registration point on the phantom;(d)Path planning by Improved-APF after registration and surgical planning; **Motion execution:**(e)On starting point;(f)On the way;(g)On the feeding point;(h)On the contacting point

point and an entry point in {C}. **Fig.12b** shows the 3D model of the phantom. With the method in Sect. 2.5, we obtained the relationship between each coordinate system and had a trajectory based on improved-APF planned (**Fig.12d**).

The robotic system moved along the trajectory generated by improved-APF (**Fig.12e**, **12f**), arriving at the feeding point (**Fig.12g**), and finally reached the contacting point with expected orientation (**Fig.12h**). When executing needle insertion, the force captured by the sensor was recorded, which is shown in **Fig.13**.

According to the force-displacement characteristics in [33], the needle experienced the event of loading deformation when contacting the skin (1→2). When the linear elastic force reached its maximum, a crack suddenly propagated into the skin, which causing a rupture event (2→3). From 2 to 3, the needle's tip cut through the skin and got into the body in 3, where also caused a loading deformation and rupture event (3→4) when contacting body tissue. When the needle reached 4, it encountered the ‘tumor’ in the phantom and experienced the event of loading deformation (4→5)

again. Then the needle stopped at the center of the ‘tumor’, which made elastic potential energy decrease slowly (5→6). From 5 to 6, the needle was experiencing the event of unloading deformation.

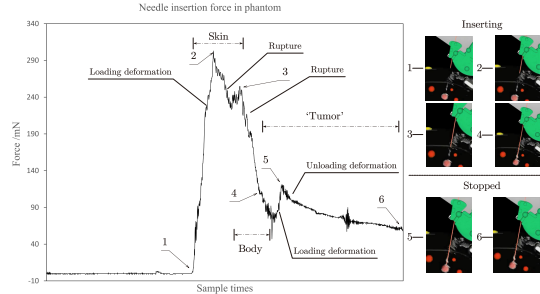


Fig. 13: Axial force suffered by needle when inserting in the phantom

#### 4 Discussion and conclusion

Radioactive seeds implantation is an effective, minimally invasive treatment method for malignant liver tumors in HCC [3]. However, the accuracy of seeds implantation, which is vital for the efficacy of the technique, is highly dependent upon surgeon experience, especially for large tumors. Large tumors require multiple needles insertion and seeds implantation to cover the whole tumor, with difficulties like obstacles in the abdomen and movement of the liver caused by breathing. Robotic systems provide surgeons with accurate needle insertion and seeds implantation under the guidance of pre-operative CT scanning, and several research groups have proposed their work in robotic system assisted needle insertion and implantation [19, 20, 21, 22, 23, 24]. However, few works have been proposed about robot-assisted radioactive seeds implantation for malignant liver tumors in HCC.

In this paper, a 7-DoF robotic system with force and US image feedback was developed for the therapy. After the calibration and surgical planning of the robotic system, it can provide a stable and accurate motion of end effector (needle guide). Besides, improved artificial potential field approach [31] was introduced into the system for avoiding collision between the robotic system and patient when executing motion. The reason we use this method is that it can be further developed under the environment of Kinect (Microsoft, USA), which can provide the algorithm with intra-operative point cloud as obstacles. The experiment results show that the robotic system is capable to execute a needle insertion task under the guidance of pre-operative CT-scanning at an acceptable accuracy. It can be used for seeds implantation of malignant tumors, including but not limited to lung cancer, head and neck cancer, pancreatic cancer [34].

Motion control of the current system assumes that the needle is a rigid body, which means the curve of it isn't taken into consideration. Substantial works have

illustrated the influence of bevel needle bending to accuracy when inserting [35, 36, 37]. Therefore, the function will be a direction in designing the next generation of the robotic system. Besides, the information from force feedback and US image hasn't been utilized sufficiently, which has been shown beneficial in the control of the needle-insertion robotic system [17, 38, 39, 40]. Nevertheless, the mechanical structure and experiments show that it is possible to further develop in the robotic system according to the problems. Meanwhile, more accuracy experiments on phantoms and in-vivo are needed to evaluate the robotic system comprehensively. In our future work, we will continuously increase the accuracy of the robotic system and conduct more experiments on phantoms and animals. We also plan to update our navigation system, where the information of force and US image will be processed and provides the operator with navigation and safety advice.

**Acknowledgements** If you'd like to thank anyone, place your comments here and remove the percent signs.

## References

1. Bray F, Ferlay J, Soerjomataram I, Siegel RL, Torre LA, Jemal A (2018) Global cancer statistics 2018: GLOBOCAN estimates of incidence and mortality worldwide for 36 cancers in 185 countries. CA: a cancer journal for clinicians 68(6):394–424, publisher: Wiley Online Library
2. Raza A, Sood GK (2014) Hepatocellular carcinoma review: current treatment, and evidence-based medicine. World journal of gastroenterology: WJG 20(15):4115, publisher: Baishideng Publishing Group Inc
3. Pollock R, Mozer P, Guzzo TJ, Marx J, Matlaga B, Petrisor D, Vigaru B, Badaan S, Stoianovici D, Allaf ME (2010) Prospects in Percutaneous Ablative Targeting: Comparison of a Computer-Assisted Navigation System and the AcuBot Robotic System. Journal of Endourology 24(8):1269–1272, DOI 10.1089/end.2009.0482, URL <http://www.liebertpub.com/doi/10.1089/end.2009.0482>
4. Qian J, Bao Z, Zou J, Yang H (2016) Effect of pedicle fixation combined with 125I seed implantation for metastatic thoracolumbar tumors. Journal of Pain Research 9:271–278, DOI 10.2147/JPR.S105284, URL <https://www.ncbi.nlm.nih.gov/pmc/articles/PMC4869845/>
5. Li JR, Sun Y, Liu L (2015) Radioactive Seed Implantation and Lobaplatin Chemotherapy Are Safe and Effective in Treating Patients with Advanced Lung Cancer. Asian Pacific Journal of Cancer Prevention 16(9):4003–4006, DOI 10.7314/APJCP.2015.16.9.4003
6. Tao H, Xiaodan Y, Ying X, Zhendong Z, Ying Y, Ning W (2017) Therapeutic value of 3-D printing template-assisted <sup>125</sup>I-seed&nbsp;implantation in the treatment of malignant liver tumors. OncoTargets and Therapy Volume 10:3277–3283, DOI 10.2147/OTT.S134290, URL <https://www.dovepress.com/therapeutic-value-of-3-d-printing-template-assisted-125i-seed-implanta-peer-reviewed-article-OTT.S134290>

7. Kettenbach J, Kronreif G (2015) Robotic systems for percutaneous needle-guided interventions. *Minimally Invasive Therapy & Allied Technologies* 24(1):45–53, publisher: Taylor & Francis
8. Zhang S, Jiang S, Yang Z, Liu R, Yunpeng Yang HL (2016) An ultrasound image navigation robotic prostate brachytherapy system based on US to MRI deformable image registration method. *Hell J Nucl Med* 19(3):223–230
9. Franco E, Ristic M (2014) Design and control of needle positioner for MRI-guided laser ablation of the liver. In: 2014 IEEE/ASME 10th International Conference on Mechatronic and Embedded Systems and Applications (MESA), IEEE, pp 1–6
10. Franco E, Brujic D, Rea M, Gedroyc WM, Ristic M (2015) Needle-guiding robot for laser ablation of liver tumors under MRI guidance. *IEEE/ASME Transactions on Mechatronics* 21(2):931–944, publisher: IEEE
11. Song SE, Tokuda J, Tuncali K, Yamada A, Torabi M, Hata N (2013) Design evaluation of a double ring RCM mechanism for robotic needle guidance in MRI-guided liver interventions. In: 2013 IEEE/RSJ International Conference on Intelligent Robots and Systems, IEEE, pp 4078–4083
12. Hata N, Tokuda J, Hurwitz S, Morikawa S (2008) MRI-compatible manipulator with remote-center-of-motion control. *Journal of Magnetic Resonance Imaging: An Official Journal of the International Society for Magnetic Resonance in Medicine* 27(5):1130–1138, publisher: Wiley Online Library
13. Sato I, Nakamura R, Masamune K (2010) MRI compatible manipulator with MRI-guided needle insertion support system. In: 2010 International Symposium on Micro-NanoMechatronics and Human Science, IEEE, pp 77–82
14. Arnolli MM, Buijze M, Franken M, de Jong KP, Brouwer DM, Broeders IA (2018) System for CT-guided needle placement in the thorax and abdomen: a design for clinical acceptability, applicability and usability. *The International Journal of Medical Robotics and Computer Assisted Surgery* 14(1):e1877, publisher: Wiley Online Library
15. Shah S, Kapoor A, Ding J, Guion P, Petrisor D, Karanian J, Pritchard WF, Stoianovici D, Wood BJ, Cleary K (2008) Robotically assisted needle driver: evaluation of safety release, force profiles, and needle spin in a swine abdominal model. *International Journal of Computer Assisted Radiology and Surgery* 3(1-2):173–179, publisher: Springer
16. Kobayashi Y, Onishi A, Watanabe H, Hoshi T, Kawamura K, Hashizume M, Fujie MG (2010) Development of an integrated needle insertion system with image guidance and deformation simulation. *Computerized Medical Imaging and Graphics* 34(1):9–18, publisher: Elsevier
17. Boctor EM, Choti MA, Burdette EC, Webster III RJ (2008) Three-dimensional ultrasound-guided robotic needle placement: an experimental evaluation. *The International Journal of Medical Robotics and Computer Assisted Surgery* 4(2):180–191, publisher: Wiley Online Library
18. Orhan SO, Yildirim MC, Bebek O (2015) Design and modeling of a parallel robot for ultrasound guided percutaneous needle interventions. In: IECON 2015 - 41st Annual Conference of the IEEE Industrial Electronics Society, IEEE, Yokohama, pp 005002–005007, DOI 10.1109/IECON.2015.7392885, URL [http:](http://)

- //ieeexplore.ieee.org/document/7392885/
- 19. Ma X, Yang Z, Jiang S, Zhang G, Chai S (2019) A novel auto-positioning method in Iodine-125 seed brachytherapy driven by preoperative planning. *Journal of applied clinical medical physics* 20(6):23–30, publisher: Wiley Online Library
  - 20. Zequn L, Chang L, Xuehe Z, Gangfeng L, Jie Z (2019) The Robot System for Brachytherapy. In: 2019 IEEE/ASME International Conference on Advanced Intelligent Mechatronics (AIM), IEEE, pp 25–29
  - 21. Ban G, Li C, Zhang X, Liu G, Liu Y, Zhao J, Zhang L, Fan Y (2019) Design of A Close-range Radiotherapy Particle Implantation Device. In: 2019 IEEE International Conference on Robotics and Biomimetics (ROBIO), IEEE, pp 1331–1337
  - 22. Zhu JH, Wang J, Wang YG, Li M, Liu XJ, Guo CB (2019) Prospect of robotic assistance for fully automated brachytherapy seed placement into skull base: Experimental validation in phantom and cadaver. *Radiotherapy and Oncology* 131:160–165, DOI 10.1016/j.radonc.2017.11.031, URL <https://linkinghub.elsevier.com/retrieve/pii/S016781401732755X>
  - 23. Zhu JH, Wang J, Wang YG, Li M, Guo YX, Liu XJ, Guo CB (2017) Performance of robotic assistance for skull base biopsy: a phantom study. *Journal of Neurological Surgery Part B: Skull Base* 78(05):385–392, publisher: Georg Thieme Verlag KG
  - 24. Jiang S, Yang Y, Yang Z, Zhang Z, Liu S (2017) Design and Experiments of Ultrasound Image-Guided Multi-DOF Robot System for Brachytherapy. *Transactions of Tianjin University* 23(5):479–487, publisher: Springer
  - 25. Hata N, Hashimoto R, Tokuda J, Morikawa S (2005) Needle guiding robot for MR-guided microwave thermotherapy of liver tumor using motorized remote-center-of-motion constraint. In: Proceedings of the 2005 IEEE International Conference on Robotics and Automation, IEEE, pp 1652–1656
  - 26. D'Onofrio M, De Robertis R, Demozzi E, Crosara S, Canestrini S, Mucelli RP (2014) Liver volumetry: Is imaging reliable? Personal experience and review of the literature. *World journal of radiology* 6(4):62, publisher: Baishideng Publishing Group Inc
  - 27. Soyer P, Sirol M, Dohan A, Gayat E, Placé V, Hristova L, Hamzi L, Boudiaf M (2012) Hepatic height on coronal computed tomography images predicts total liver volume in European adults without liver disease. *Digestive diseases and sciences* 57(6):1692–1697, publisher: Springer
  - 28. Hager DA, Nyland TG, Fisher P (1985) Ultrasound-guided biopsy of the canine liver, kidney, and prostate. *Veterinary Radiology* 26(3):82–88, publisher: Wiley Online Library
  - 29. Craig JJ (2005) Introduction to Robotics
  - 30. Day M, Games I (2012) Extracting Euler angles from a rotation matrix. Insomniac Games R&D Available online at: <http://www.insomniacgames.com/mike-day-extracting-euler-angles-from-a-rotation-matrix>
  - 31. Ge SS, Cui YJ (2000) New potential functions for mobile robot path planning. *IEEE Transactions on robotics and automation* 16(5):615–620, publisher: IEEE
  - 32. Besl P, McKay ND (1992) A method for registration of 3-D shapes. *IEEE Transactions on Pattern Analysis and Machine Intelligence* 14(2):239–256, DOI 10.1109/34.121791, conference Name: IEEE Transactions on Pattern Analysis

- and Machine Intelligence
- 33. Mahvash M, Dupont PE (2009) Mechanics of dynamic needle insertion into a biological material. *IEEE Transactions on Biomedical Engineering* 57(4):934–943
  - 34. Liu Y, Liu R, Wang P, Li S, Shen H (2015) Percutaneous implantation of 125 iodine seeds for treatment of portal vein tumor thrombosis in hepatocellular carcinoma. *Medical Oncology* 32(8):214
  - 35. Meltsner M, Ferrier N, Thomadsen B (2007) Observations on rotating needle insertions using a brachytherapy robot. *Physics in Medicine & Biology* 52(19):6027
  - 36. Misra S, Reed KB, Schafer BW, Ramesh K, Okamura AM (2010) Mechanics of flexible needles robotically steered through soft tissue. *The International journal of robotics research* 29(13):1640–1660
  - 37. Khadem M, Rossa C, Usmani N, Sloboda RS, Tavakoli M (2016) A two-body rigid/flexible model of needle steering dynamics in soft tissue. *IEEE/ASME Transactions on Mechatronics* 21(5):2352–2364
  - 38. Chevrie J, Krupa A, Babel M (2019) Real-time teleoperation of flexible beveled-tip needle insertion using haptic force feedback and 3d ultrasound guidance. In: 2019 International Conference on Robotics and Automation (ICRA), IEEE, pp 2700–2706
  - 39. Pacchierotti C, Abayazid M, Misra S, Prattichizzo D (2014) Teleoperation of steerable flexible needles by combining kinesthetic and vibratory feedback. *IEEE transactions on haptics* 7(4):551–556
  - 40. Kobayashi Y, Onishi A, Watanabe H, Hoshi T, Kawamura K, Hashizume M, Fujie MG (2010) Development of an integrated needle insertion system with image guidance and deformation simulation. *Computerized Medical Imaging and Graphics* 34(1):9–18